https://doi.org/10.3311/PPme.20382

Periodica Polytechnica Mechanical Engineering

A Study on the Shape and Dimensional Accuracy of Additively Manufactured Titanium Lattice Structures for Orthopedic Purposes

Rashwan Alkentar[1,2*], Tamás Mankovits[2]

[1] Doctoral School of Informatics, Faculty of Informatics, University of Debrecen, Ótemető Street 2-4, H-4028 Debrecen, Hungary
[2] Department of Mechanical Engineering, Faculty of Engineering, University of Debrecen, Ótemető street 2-4., H-4028 Debrecen, Hungary
* Corresponding author, e-mail: rashwan.alkentar@eng.unideb.hu

Received: 27 April 2022, Accepted: 15 September 2022, Published online: 20 September 2022

Abstract

The deviation between the designed lattice structures and the 3D-printed ones has been studied in this research. Three types of lattice structures were designed using the SpaceClaim application in the ANSYS software and then fabricated using Direct Metal Laser Sintering (DMLS) via EOS M 290 3D printer. Considering the orthopedic application, Ti6Al4V alloy of grade 23 was selected as a material for all samples of the structures. A thorough comparison was done on the volume, mass, and porosity to effectively map the possible deviations between the designed and the printed version. The shape accuracy of the 3D printing process was discussed during the study. As the complexity of the shape of the unit cell increases, the accuracy of the printing process becomes lower. Dimensional accuracy in the XY plane is higher than accuracy in the Z plane. Simple unit cell shape was proven to be more accurate in the 3D printing process.

Keywords

3D printing, lattice structures, dimensional accuracy

1 Introduction

Lattice structures can be explained as three-dimensional structures composed in topological order and composed of one or more repeated unit cells [1, 2]. The effective mechanical properties of such structures can be changed by adjusting parameters to show better properties than those of the original material. In the biomedical field, lattice structures are good solutions to diminish the stiffness of the metal prosthesis and get it as close as possible to the stiffness of the bone [3], thus avoiding the stress shielding effect [4]. Since the lattice structure achieves a high surface area-to-volume range, it facilitates better osseointegration [5].

As the parameters (beam's thickness, diameter, cross, etc.) of the latticed structures have a huge effect on how they react against mechanical loads (e.g. on the mechanical properties), the accuracy of modeling them became inevitable. Recent researches rely on computer-aided design (CAD) software to model the lattice structures [6, 7]. Usually, the software dedicates a library of unit cells. The unit cells are copied to produce the lattice structure, and the latticing of large-scale structures requires heavy-duty computer resources [8, 9]. Therefore, MATLAB is used to develop a routine for modeling the lattice structure and exporting an STL file ready for additive manufacturing (AM), as reported in [10].

In order to develop better latticed structures, many researches have been conducted and reported recently. Hollister [11], created lattice structures with good properties using an image-based approach where the data were taken out of patient-specific medical imaging. Fryazinov et al. [12] and Yoo [13], proposed the application of implicit functions for the purpose of modelling structures in compact form. The control of the parameters of the structures is easier using this method, by simply adjusting the underlying functions. The obvious disadvantage here is the additional processing needed to convert the files to STL format for AM manufacturing.

The next critical point is the production of the lattice structure by 3D printing, where the main job of additive manufacturing is to attain high shape and dimensional accuracy and good repeatability of the fabricated parts [14].

Cite this article as: Alkentar, R., Mankovits, T. "A Study on the Shape and Dimensional Accuracy of Additively Manufactured Titanium Lattice Structures for Orthopedic Purposes", Periodica Polytechnica Mechanical Engineering, 2022. https://doi.org/10.3311/PPme.20382

Metallic lattice structures with small-diameter struts are fabricated using Laser Powder Bed Fusion (LPBF) [15], especially TiNi alloys, and Selective Laser Melting (SLM) [16]. Qiu et al. [17], proved that the printed structures showed higher values of deviation in the diameter of the strut with the increase in laser power used in printing.

However, these two methods are still the most common ways of manufacturing techniques of the AM used for producing lattice structures. CAD data are taken in order to manufacture the metallic components using layer by layer fusion with laser energy [18]. PBF methods are preferred due to their efficiency and accuracy when compared to other AM methods like direct metal deposition [1].

Controlling the parameters of the printing process of the PBF techniques plays a significant role in defining the final properties of the structures. In the study of Tan et al. [15], the parameters were adjusted and recorded where they showed the obvious effect of changing the laser power, hatch space and the printing orientation on the mechanical properties of the lattice structures [19]. Another good and reliable PBF-based AM method is the Direct Metal Laser Sintering (DMLS). In the research of Yan et al. [20], the mechanical properties of periodic cellular lattice structures were investigated for many unit cell sizes fabricated using the DMLS technique. The research showed that the bigger the unit cell size was, the less the compression strength became, provided that the volume fraction is fixed.

In the current research, the focus is on the determination of the deviation between the designed unit cells and the manufactured ones with discussing the reasons behind them. The ANSYS SpaceClaim application was used for the geometry design and generating of the STL file and the 3D printing was done by the DMLS method via an EOS M 290 machine.

2 Materials and methods

2.1 Raw material

Titanium alloys were extensively used for decades for the fabrication of biomedical devices. Ti6Al4V alloy of grade 23 supplied by EOS Gmbh was used in printing the structures. The material is famous for its good mechanical properties, especially low density, high strength and high corrosion resistance that are advantageous in the aspects of better osseointegration and biocompatibility. Table 1 shows the chemical composition of the Ti6Al4V grade 23 alloy used in the study [21].

Table 1 Chemical composition of the Ti6Al4V grade 23 alloy

Element	Chemical Composition Percentage %
Al	5.50–6.50
V	3.50–4.50
O	0.13
N	0.05
C	0.08
H	0.012
Fe	0.25
Y	0.005
Other elements each	0.1
Other elements total	0.4

2.2 Lattice design

Three types of latticed structures were designed using the SpaceClaim application within the ANSYS software 2020 R2 version. The original bulk dimensions of the specimens before applying the lattice optimization are 20 × 20 × 30 mm with a squared cross-section. The shell command in the SpaceClaim application offers various shapes of basic latticed infills. Two main variables are used to define the filling percentage and generate the desired optimized structure:

- length (distance between the centers of each unit cell)
- strut thickness.

The lattice optimization was applied on 20 mm of the height of the specimen, thus leaving 5 mm from the top and bottom of the specimen as shown in Fig. 1. The variables were chosen based on the idea of having a close-in-value filling percentage for all three types of specimens

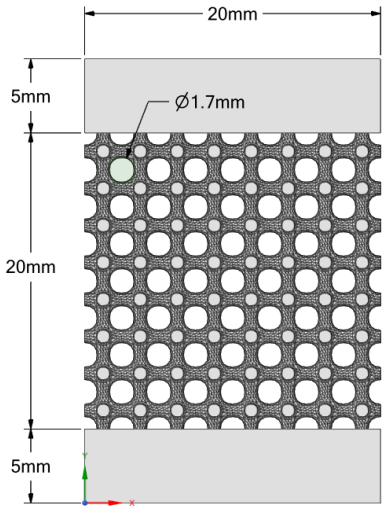

Fig. 1 Model dimensions of the specimen

to make sure the comparison is as effective as possible by having a small range of porosity percentages for all three types. ISO 13314:2011 [22] standard was followed in terms of the relations among dimensions where the length width and height of each unit cell are equal to or more than ten times the size of the pore size. Fig. 2 shows the 3D-printed specimens with dimensions.

Table 2 shows the chosen shapes of the unit cells to be applied and the related variables.

The unit cells after the lattice optimization application are shown in Fig. 3 to better view the geometry of each lattice type.

The full CAD models, 20 × 20 × 30 mm sized models, of the specimens were generated via the SpaceClaim and then converted into STL format to be ready for manufacturing via AM.

Since the effect of the porosity of the specimens on their properties is high, the porosity percentage calculation was done for each specimen using the following Eq. (1). The porosity of the structure was calculated for the latticed part with Eq. (1):

$$\phi(\%) = \frac{V_{\text{bulk}} - V_{\text{lattice}}}{V_{\text{bulk}}} \times 100\,, \tag{1}$$

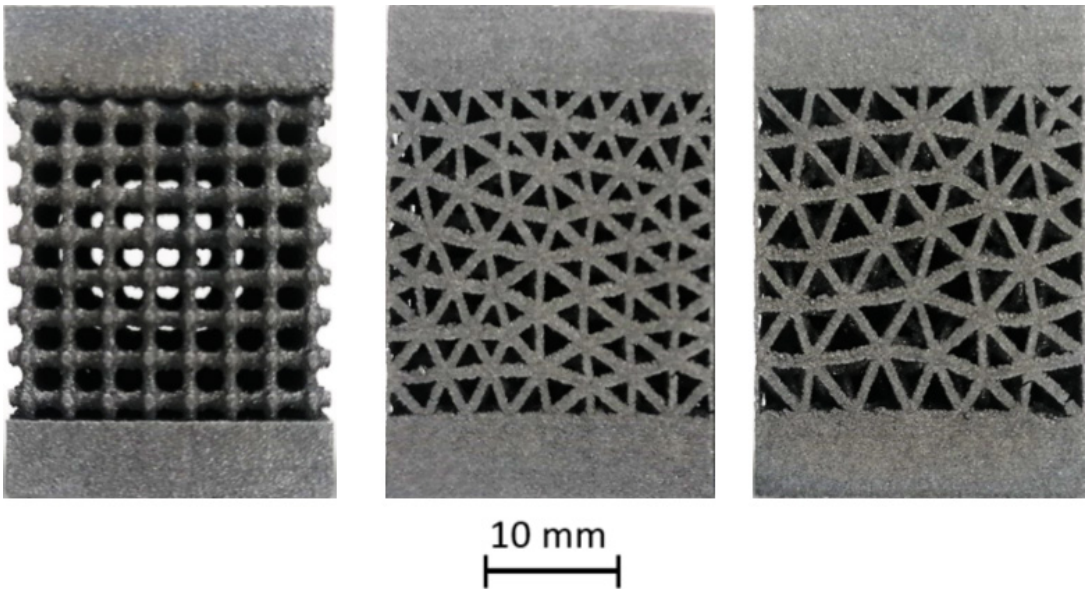

(a) (b) (c)

Fig. 2 The 3D printed specimens: (a) 3 Dimensional Lattice Infill Pattern, (b) Double pyramid lattice with face diagonals, (c) Octahedral lattice 2

Table 2 Parameters of the lattice optimization

Unit cell type	Thickness (mm)	Length (mm)
3 Dimensional Lattice Infill Pattern	0.7	1.8
Double pyramid lattice with face diagonals	0.7	3.5
Octahedral lattice 2	0.7	3.8

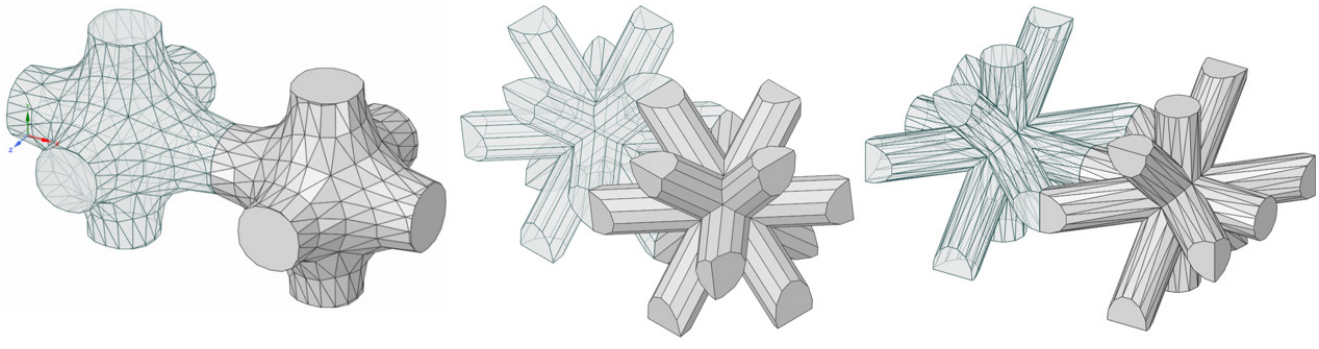

(a) (b) (c)

Fig. 3 The geometrical shape of the unit cell: (a) 3 Dimensional Lattice Infill Pattern, (b) Double pyramid lattice with face diagonals, (c) Octahedral lattice 2

where ϕ is the porosity, $V_{lattice}$ is the volume of the latticed structure, and V_{bulk} is the bulk volume (to be latticed) of the specimen which is a constant value of 8000 mm. The weight of each specimen was then calculated using Eq. (2) with the help of the material density of 4.43 g/cm^3 to determine the difference between the designed weight and the printed weight:

$$\rho = \frac{m}{V}, \tag{2}$$

where ρ is the density (g/cm^3), m is the mass of the specimen (g), and V is the volume of the specimen (mm). The numeric calculations are to be compared with those of the manufactured specimens. As for the volumes of the printed samples, they can be calculated using the same Eq. (2), by dividing the mass of the printed sample over the density of the alloy used. The porosity of the printed samples, then, can be calculated with the same Eq. (1) considering the V_{bulk} to be the volume calculated from the dimensions of the printed samples, and the $V_{lattice}$ to be the volume calculated based on the mass from Eq. (2).

2.3 The manufacturing process

The printing process was done using the DMLS method. EOS M 290 machine was used to 3D-print the specimens. The laser type in the printing is a Yb fiber laser with a power of 400 W. The scanning speed of the machine is 7 m/s with a focus diameter of 100 µm [23]. The machine uses EOSPRINT 2 software that enables the optimization of the CAD data inserted. Six samples of each type were manufactured.

2.4 Scanning

Scanning was executed for the specimens to run further investigation on the accuracy of the printing process. GOM ATOS high-speed scanning system was used to perform the scanning operation. The scanning includes precise measurement with detailed resolution using structured blue light [24]. The printed specimens were then compared with the CAD STEP file to show the deviation graphically.

3 Results

3.1 CAD model properties

Using the SpaceClaim measurement features, the calculations for the numeric model were done. The volume of the specimen was taken from the software. Porosity and mass were calculated using Eq. (1) and Eq. (2). The porosity calculation was mainly considered for the latticed part. Table 3 shows the nominal details. The values of the measurements and the calculations were considered nominal values to run a comparison with the results of the manufactured samples.

3.2 Manufactured unit cells properties

The manufactured specimens were measured in terms of dimensions, masses, volumes and porosities to be compared with the nominal values of the numerical model. A digital caliper of type Mitutoyo with a precision of ±0.02 mm was used to measure the dimensions, and a scale of type Ohaus Navigator with 0.01 g readability was used to weigh the specimens. The mean and standard deviation have been calculated for all six specimens of each type. The calculated mean was then compared with the nominal mean value taken from the designed model to check the deviation percentage.

Table 4 shows the average of the measurements and the deviation from the nominal values for all three types of specimens. For the 3D lattice infill type, the maximum deviation in terms of dimensions is visible in the height with a percentage of 1.15%. The mass deviation is a little bit higher with a maximum percentage of 1.89%. The inaccuracy in the 3D printing caused a decrease in the length and width, however, added extra height leading to an average shortage in the mass of up to 0.32 g. The double pyramid lattice with face diagonals type shows a deviation in length close to the previous case with a percentage of 0.36%, whereas the deviation in the width is of a higher percentage of 0.63%. The deviation in the mass reaches 1.6%, which is less than the case of the 3D lattice infill type. For the octahedral lattice 2 type of specimens, it is obvious that the deviation percentages are higher than the rest of the types. The deviation in the mass is up to 2.03% of the designed value, which is the highest value among all three types. However, the dimensions deviation is close to the rest of the types with only the width being higher reaching 0.8%.

Fig. 4 exhibits the variance and the relative error in dimensions among the six specimens of the three types of the lattice structure.

Table 3 Numerical details from the CAD models

Unit cell type	Volume (mm)	Mass (g)	Porosity (%)
3 Dimensional Lattice Infill Pattern	2079.18	26.93	74.0
Double pyramid lattice with face diagonals	2480.47	28.70	69.0
Octahedral lattice 2	2550.91	29.00	68.4

Table 4 Comparison between measurements and numerical data for all three latticed structure types

Specimen	Length (mm)	Width (mm)	Height (mm)	Mass (g)
3 Dimensional Lattice Infill Pattern				
Mean (specimens)	19.99	19.97	30.29	26.61
Std. Deviation	0.04	0.03	0.05	0.14
Nominal Mean (CAD model)	20.00	20.00	30.00	26.93
Error (Nominal, Specimens)	0.01	0.03	0.29	0.32
Max deviation	0.080	0.060	0.347	0.510
Max deviation percentage (%)	0.400	0.300	1.156	1.894
Double pyramid lattice with face diagonals				
Mean (specimens)	19.96	20.03	30.24	28.34
Std. Deviation	0.04	0.06	0.03	0.10
Nominal Mean (CAD model)	20.00	20.00	30.00	28.70
Error (Nominal, Specimens)	0.04	0.03	0.24	0.37
Max deviation	0.073	0.127	0.273	0.460
Max deviation percentage (%)	0.367	0.633	0.911	1.602
Octahedral lattice 2				
Mean (specimens)	20.04	20.03	30.26	28.44
Std. Deviation	0.07	0.08	0.06	0.04
Nominal Mean (CAD model)	20.00	20.00	30.00	29.00
Error (Nominal, Specimens)	0.04	0.03	0.26	0.58
Max deviation	0.133	0.163	0.333	0.590
Max deviation percentage (%)	0.667	0.817	1.111	2.033

Based on the presented results, the 2D dimensional accuracy along the XY-axis was higher than on the Z-axis where the overall length and width reached a maximum deviation of 0.8%, and the overall height reached a maximum deviation of 1.15%.

If the average masses and the nominal ones are plotted, as seen in Fig. 5, it is clear how the deviation is the highest in the octahedral lattice 2 type out of the group. These results are due to the octahedral lattice 2 type being the most complicated shape of all the types. The inaccuracy, however, within the 3D printing process may come from all the participating factors: the machine accuracy (laser power, printing bed's movement ... etc.), the material quality, and the object size.

Table 5 lists both the volumes calculated based on the dimensions of the latticed part of the printed samples, and the volumes calculated based on the weighed mass of each sample. In terms of the maximum deviation, the octahedral lattice 2 type shows the highest percentage up to 5.4% in volume, whereas the rest two types show close results.

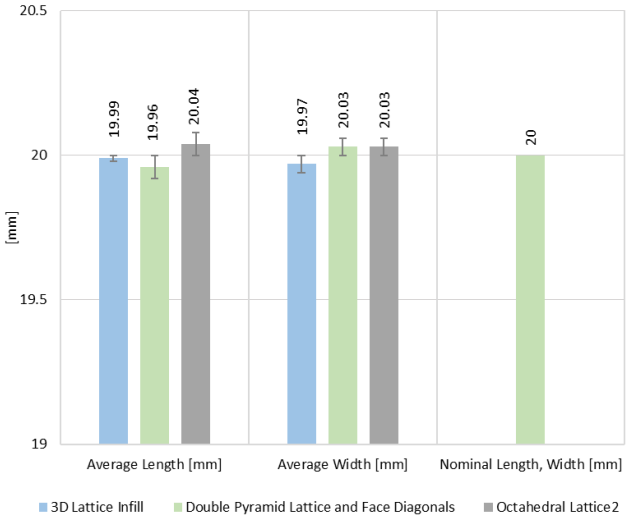

(a)

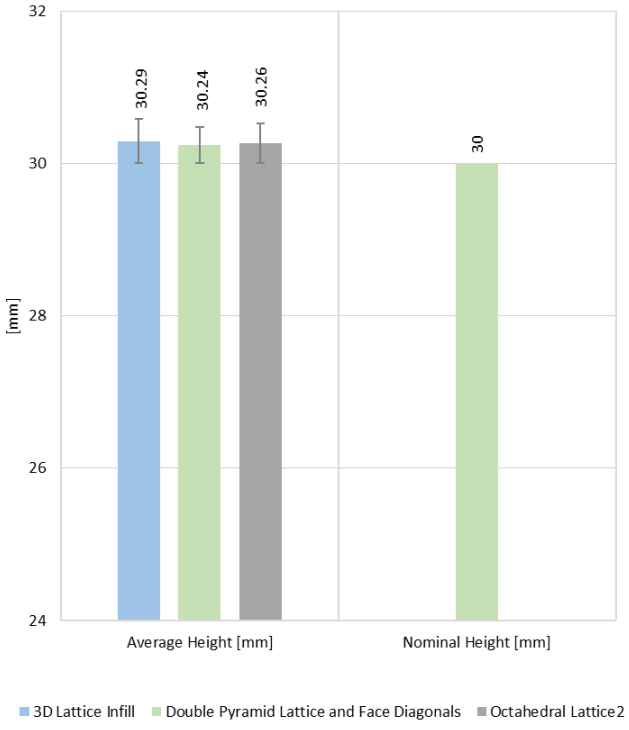

(b)

Fig. 4 Variance and measurement details among the dimensions of all three latticed structure types (a) Variance of the length and width, (b) Variance of the height

For the porosity results, Table 6 shows the porosity values and the percentages in deviation. As above-mentioned, the total bulk volume was calculated using the measured dimensions of the printed samples, and the latticed volume was calculated using Eq. (1).

Fig. 6 shows a graphic comparison among all the types in terms of porosity where it is clear that the octahedral lattice 2 has the highest deviation of 2.93% from the

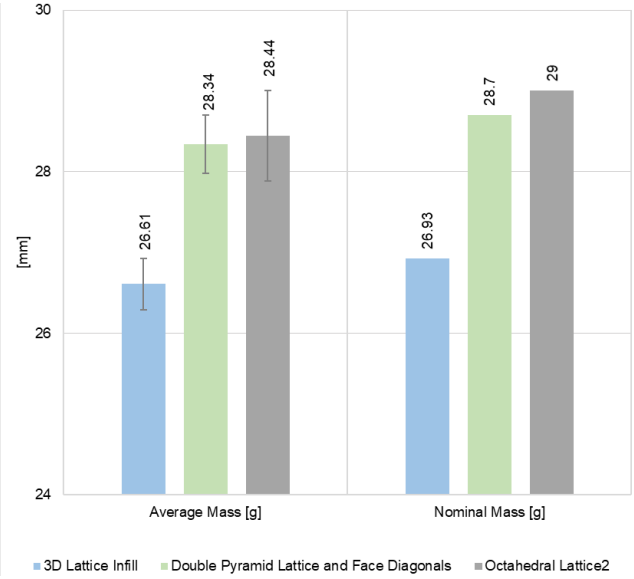

Fig. 5 The variance and relative errors of masses within the three types of specimens

Table 5 The volume calculation and variance for the latticed part

Specimen	3D Lattice Infill Pattern	Double pyramid lattice with face diagonals	Octahedral lattice 2
Mean Volume (mm)	2009.78	2396.91	2420.24
Std. Volume (mm)	27.67	22.86	8.38
Nominal CAD volume (mm)	2079.18	2480.48	2550.91
Error (Nominal, Specimens)	69.40	83.56	130.67
Deviation percentage (%)	3.34	3.37	5.12
Max deviation percentage (%)	4.79	4.26	5.40

Table 6 The porosity calculation and variance

Specimen	3D Lattice Infill Pattern	Double pyramid lattice with face diagonals	Octahedral lattice 2
Mean porosity(specimens) %	75.18	70.39	70.23
Std. porosity(specimens) %	0.37	0.23	0.16
Nominal CAD porosity %	74	69	68.4
Error (Nominal, Specimens)	1.183	1.394	1.835
Deviation percentage %	1.60	2.02	2.68
Max deviation	1.72	1.74	2.00
Max deviation percentage (%)	2.33	2.52	2.93

designed value. The other two types have shown similar results around 2% maximum deviation.

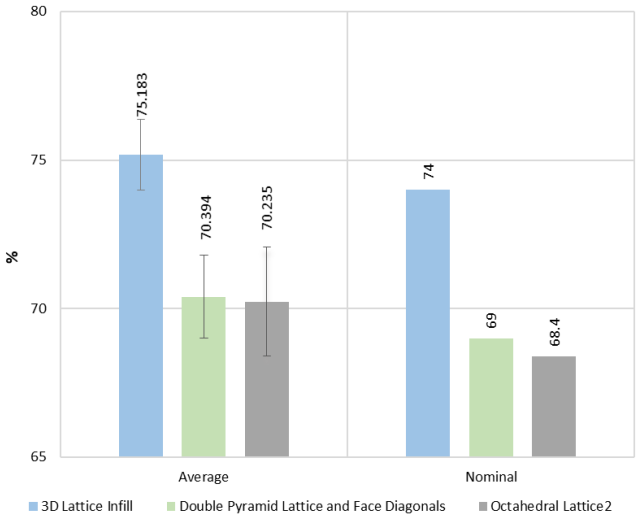

Fig. 6 Porosity comparison among all types of lattice structures

3.3 Scanning

For the sake of the accuracy investigation, the specimens were scanned to be compared with the CAD file. Fig. 7 shows the results of the scanning where the green areas represent that the material distribution is appropriate, while the red areas represent the existence of too much material, and the blue areas mean the lack of material.

Since the relevance between the material distribution and the accuracy at the dimensional level, the representation shown in the Fig. 7 is compared with the dimensional accuracy graph. The accuracy level range varies by ±0.15 mm. The fluctuations in the graph of the material distribution seen in the octahedral lattice 2 type agree with the results of dimensional accuracy presented before, which proves the complexity of the shape to be a vital reason for having inaccurate results.

It is noticed that the excess of material is mainly seen in the connection areas between the latticed part and the bulk part. The change in the amount of material on the connection plane caused the extra precipitations, especially when building in an area with no material beneath.

4 Conclusions

The research studied three types of latticed structures to conduct a comparison between the designed structures and the manufactured ones. The shapes of the unit cell applied to get the lattice optimization were presented. Six samples of each specimen type were 3D printed using the EOS M 290 machine that uses the DMLS method for manufacturing. Ti6Al4V alloy of grade 23 was used as a material for all specimens. The major findings of the research are:

1. The 3D printing accuracy in the XY direction is noticed to be higher than the accuracy in the Z direction which relates to the accuracy of the machine.

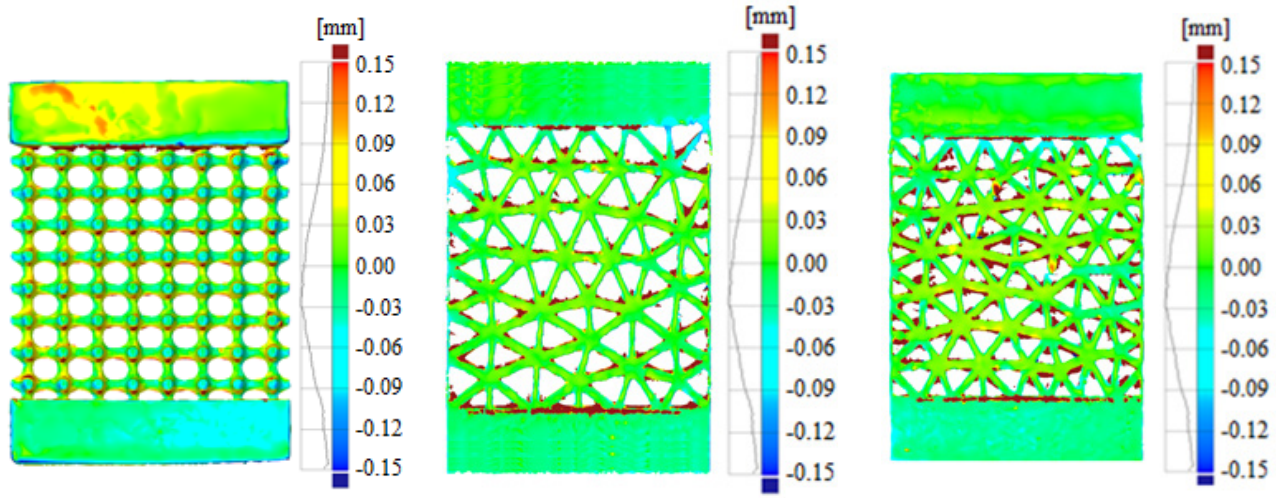

(a) (b) (c)

Fig. 7 Surface deviation plot for all three types of specimens: (a) 3 Dimensional Lattice Infill Pattern, (b) Double pyramid lattice with face diagonals, (c) Octahedral lattice 2

2. The more complex the shape of the structure being printed is, the less accurate results the machine generates.
3. As the size of the objects to be printed increases, the accuracy of the process decreases. This finding might be connected to the machine's accuracy over the production time.
4. In terms of accuracy, it is recommended to use a simple structure unit cell shape (3D lattice infill type for example), however, further tests are needed to compare the mechanical properties resulting from each shape.
5. Based on the 3D scanning and inspection, there is some fluctuation in the distribution of the material. The accuracy of the material distribution is influenced by the direction of laser scanning while printing, the laser power used and the scanning speed [25].

References

[1] Zadpoor, A. A. "Mechanical performance of additively manufactured meta-biomaterials", Acta Biomaterialia, 85, pp. 41–59, 2019. https://doi.org/10.1016/j.actbio.2018.12.038

[2] Zhang, X. Z., Leary, M., Tang, H. P., Song, T., Qian, M. "Selective electron beam manufactured Ti-6Al-4V lattice structures for orthopedic implant applications: Current status and outstanding challenges", Current Opinion in Solid State and Materials Science, 22(3), pp. 75–99, 2018. https://doi.org/10.1016/j.cossms.2018.05.002

[3] Alabort, E., Barba, D., Reed, R. C. "Design of metallic bone by additive manufacturing", Scripta Materialia, 164, pp. 110–114, 2019. https://doi.org/10.1016/j.scriptamat.2019.01.022

[4] Zargarian, A., Esfahanian, M., Kadkhodapour, J., Ziaei-Rad, S., Zamani, D. "On the fatigue behavior of additive manufactured lattice structures", Theoretical and Applied Fracture Mechanics, 100, pp. 225–232, 2019. https://doi.org/10.1016/j.tafmec.2019.01.012

[5] Bici, M., Brischetto, S., Campana, F., Ferro, C. G., Seclì, C., Varetti, S., Maggiore, P., Mazza, A. "Development of a multifunctional panel for aerospace use through SLM additive manufacturing", Procedia CIRP, 67, pp. 215–220, 2018. https://doi.org/10.1016/j.procir.2017.12.202

[6] Wang, X., Xu, S., Zhou, S., Xu, W., Leary, M., Choong, P., Qian, M., Brandt, M., Xie, Y. M. "Topological design and additive manufacturing of porous metals for bone scaffolds and orthopaedic implants: A review", Biomaterials, 83, pp. 127–141, 2016. https://doi.org/10.1016/j.biomaterials.2016.01.012

[7] Giannitelli, S. M., Accoto, D., Trombetta, M., Rainer, A. "Current trends in the design of scaffolds for computer-aided tissue engineering", Acta Biomaterialia, 10(2), pp. 580–594, 2014. https://doi.org/10.1016/j.actbio.2013.10.024

[8] Papazetis, G., Vosniakos, G.-C. "Direct porous structure generation of tissue engineering scaffolds for layer-based additive manufacturing", The International Journal of Advanced Manufacturing Technology, 86(1–4), pp. 871–883, 2016. https://doi.org/10.1007/s00170-015-8237-1

[9] Medeiros e Sá, A., Mello, V. M., Rodriguez Echavarria, K., Covill, D. "Adaptive voids", The Visual Computer, 31(6–8), pp. 799–808, 2015. https://doi.org/10.1007/s00371-015-1109-8

[10] Dumas, M., Terriault, P., Brailovski, V. "Modelling and characterization of a porosity graded lattice structure for additively manufactured biomaterials", Materials & Design, 121, pp. 383–392, 2017. https://doi.org/10.1016/j.matdes.2017.02.021

[11] Hollister, S. J. "Porous scaffold design for tissue engineering", Nature Materials, 4(7), pp. 518–524, 2005. https://doi.org/10.1038/nmat1421

[12] Fryazinov, O., Vilbrandt, T., Pasko, A. "Multi-scale space-variant FRep cellular structures", Computer-Aided Design, 45(1), pp. 26–34, 2013. https://doi.org/10.1016/j.cad.2011.09.007

[13] Yoo, D.-J. "Recent trends and challenges in computer-aided design of additive manufacturing-based biomimetic scaffolds and bioartificial organs", International Journal of Precision Engineering and Manufacturing, 15(10), pp. 2205–2217, 2014. https://doi.org/10.1007/s12541-014-0583-7

[14] Farzadi, A., Solati-Hashjin, M., Asadi-Eydivand, M., Abu Osman, N. A. "Effect of Layer Thickness and Printing Orientation on Mechanical Properties and Dimensional Accuracy of 3D Printed Porous Samples for Bone Tissue Engineering", PLoS One, 9(9), e108252, 2014. https://doi.org/10.1371/journal.pone.0108252

[15] Tan, C., Li, S., Essa, K., Jamshidi, P., Zhou, K., Ma, W., Attallah, M. M. "Laser Powder Bed Fusion of Ti-rich TiNi lattice structures: Process optimisation, geometrical integrity, and phase transformations", International Journal of Machine Tools and Manufacturing, 141, pp. 19–29, 2019. https://doi.org/10.1016/j.ijmachtools.2019.04.002

[16] Essa, K., Hassanin, H., Attallah, M. M., Adkins, N. J., Musker, A. J., Roberts, G. T., Tenev, N., Smith, M. "Development and testing of an additively manufactured monolithic catalyst bed for HTP thruster applications", Applied Catalysis A: General, 542, pp. 125–135, 2017. https://doi.org/10.1016/j.apcata.2017.05.019

[17] Qiu, C., Yue, S., Adkins, N. J. E., Ward, M., Hassanin, H., Lee, P. D., Withers, P. J., Attallah, M. M. "Influence of processing conditions on strut structure and compressive properties of cellular lattice structures fabricated by selective laser melting", Materials Science and Engineering: A, 628, pp. 188–197, 2015. https://doi.org/10.1016/j.msea.2015.01.031

[18] Gong, H., Rafi, K., Gu, H., Starr, T., Stucker, B. "Analysis of defect generation in Ti–6Al–4V parts made using powder bed fusion additive manufacturing processes", Additive Manufacturing, 1–4, pp. 87–98, 2014. https://doi.org/10.1016/j.addma.2014.08.002

[19] Liverani, E., Toschi, S., Ceschini, L., Fortunato, A. "Effect of selective laser melting (SLM) process parameters on microstructure and mechanical properties of 316L austenitic stainless steel", Journal of Materials Processing Technology, 249, pp. 255–263, 2017. https://doi.org/10.1016/j.jmatprotec.2017.05.042

[20] Yan, C., Hao, L., Hussein, A., Young, P., Huang, J., Zhu, W. "Microstructure and mechanical properties of aluminium alloy cellular lattice structures manufactured by direct metal laser sintering", Materials Science and Engineering: A, 628, pp. 238–246, 2015. https://doi.org/10.1016/j.msea.2015.01.063

[21] EOS GmbH "EOS Titanium Ti64 - Material data sheet", 2017. [online] Available at: https://www.eos.info/material-m [Accessed: 25 June 2022]

[22] International Organization for Standardization " ISO 13314:2011 Mechanical testing of metals — Ductility testing — Compression test for porous and cellular metals", ISO, Geneva, Switzerland, 2011.

[23] EOS GmbH "Technical Data EOS M 290", 2022. [online] Available at: https://www.eos.info/en/additive-manufacturing/3d-printing-metal/eos-metal-systems/eos-m-290 [Accessed: 25 June 2022]

[24] GOM Metrology "Industrial 3D Measuring Systems with High-Speed Technology", [online] Available at: https://www.gom.com/en/products/high-precision-3d-metrology [Accessed: 30 March 2022]

[25] Kumar, P., Chakravarthy, P., Manwatkar, S. K., Narayana Murty, S. V. S. "Effect of Scan Speed and Laser Power on the Nature of Defects, Microstructures and Microhardness of 3D-Printed Inconel 718 Alloy", Journal of Materials Engineering and Performance, 30(9), pp. 7057–7070, 2021. https://doi.org/10.1007/s11665-021-06163-8